



# A stable ultrastructural pattern despite variable cell size in *Lithothamnion corallioides*

Valentina Alice Bracchi, Giulia Piazza, and Daniela Basso

Department of Earth and Environmental Sciences, University of Milano-Bicocca, Milan, 20126, Italy

**Correspondence:** Valentina Alice Bracchi (valentina.bracchi@unimib.it)

Received: 28 May 2021 – Discussion started: 3 August 2021

Revised: 18 October 2021 – Accepted: 20 October 2021 – Published: 25 November 2021

**Abstract.** Recent advances on the mechanism and pattern of calcification in coralline algae led to contradictory conclusions. The evidence of a biologically controlled calcification process, resulting in distinctive patterns at the scale of family, was observed. However, the coralline calcification process has been also interpreted as biologically induced because of the dependency of its elemental composition on environmental variables. To clarify the matter, five collections of *Lithothamnion corallioides* from the Atlantic Ocean and the Mediterranean Sea, across a wide depth range (12–66 m), have been analyzed for morphology, anatomy and cell wall crystal patterns in both perithallial and epithallial cells to detect possible ultrastructural changes. *L. corallioides* shows the alternation of tiers of short-squared and long-ovoid/rectangular cells along the perithallus, forming a typical banding. The perithallial cell length decreases according to water depth and growth rate, whereas the diameter remains constant. Our observations confirm that both epithallial and perithallial cells show primary (PW) and secondary (SW) calcite walls. Rectangular tiles, with the long axis parallel to the cell membrane forming a multi-layered structure, characterize the PW. Flattened squared bricks characterize the SW, with roundish outlines enveloping the cell and showing a zigzag and cross orientation. Long and short cells have different thicknesses of PW and SW, increasing in short cells. Epithallial cells are one to three flared cells with the same shape of the PW and SW crystals. Despite the diverse seafloor environments and the variable *L. corallioides* growth rate, the cell walls maintain a consistent ultrastructural pattern with unaffected crystal shape and arrangement. A comparison with two congeneric species, *L. minervae* and *L. valens*, showed similar ultrastructural patterns in the SW but evident differences in the PW crystal shape. Our observa-

tions point to a biological control rather than an induction of the calcification process in coralline algae and suggest a possible new morphological diagnostic tool for species identification, with relevant importance for paleontological applications. Finally, secondary calcite, in the form of dogtooth crystals that fill the cell lumen, has been observed. It represents a form of early alteration in living collections which can have implications in the reliability of climate and paleoclimate studies based on geochemical techniques.

## 1 Introduction

The subclass Corallinophycidae is spread globally and comprises the crustose coralline algae (CCA), important Mg-calcite calcifiers and habitat builders of rhodolith beds, temperate algal reefs and tropical coralline reefs (Adey, 1986; Cabioch and Giraud, 1986; Ries, 2006; Caragnano et al., 2009; Bracchi et al., 2014, 2016; Marchese et al., 2020). The complex calcifying process in CCA takes place during their whole life span and involves the entire organism. For this reason, corallines bear witness to past benthic primary production by macroalgae with an excellent fossil record (Basso et al., 2007; Bracchi et al., 2014, 2016; Ragazzola et al., 2020).

Rhodoliths are unattached nodules formed mostly by CCA. Among them, free-living unattached branches usually characterize maerl beds in the northeastern Atlantic Ocean (Henrich et al., 1995; Birkett et al., 1998; Peña and Bárbara, 2008, 2009; Peña et al., 2014) and in the Mediterranean Sea (Huvé, 1956; Jacquotte, 1962; Gambi et al., 2009; Agnesi et al., 2011; Savini et al., 2012; Basso et al., 2017).

In both geographical settings, the most common species are *Lithothamnion corallioides* (P. Crouan and H. Crouan)

P. Crouan and H. Crouan 1867 and *Phymatolithon calcareum* (Pallas) W. H. Adey and D. L. McKibbin ex Woelkerling and L. M. Irvine 1986 (Adey and McKibbin, 1970; Basso et al., 2017; Hernandez-Kantun et al., 2017).

*L. corallioides* is distributed between the Canary Islands, at roughly 28° N, and Scotland, at about 58° N (Irvine and Chamberlain, 1994; Wilson et al., 2004), and it is considered one of the most suitable species for paleoclimate reconstruction (Foster, 2001). This species usually forms twig-like structures and is brown to pink or purplish and often sterile, with branch diameters typically in the range of 1–2 mm and with knob-like apices (Irvine and Chamberlain, 1994). Primary production, respiration and calcification in *L. corallioides* are strongly influenced by seasonality because of the oscillations of temperature and irradiance levels (Adey and McKibbin, 1970; Potin et al., 1990; Martin et al., 2006). *L. corallioides* shows a favorable response to temperature increase, reaching its maximum primary production during summer (Adey and McKibbin, 1970; Potin et al., 1990). *L. corallioides*' minimum survival temperature is between 2 and 5 °C, while the optimal growth is observed between 13 °C (Adey and McKibbin, 1970) and 14 °C (Blake and Maggs, 2003). In longitudinal sections, the periodical change in growth rate due to the alternation of seasons generates perithallus banding in *Lithothamnion* species, as in the long protuberances of *L. corallioides*. Banding results from an evident alternation of tiers of thick-walled, generally short cells versus thin-walled long cells along the main axis of perithallus growth (Basso, 1995; Basso et al., 1997; Kamenos and Law, 2010, Burdett et al., 2011). Banding has been interpreted as the visible effect of the environment (primarily temperature) on algal growth at different timescales (day, month) (Halfar et al., 2000; Foster, 2001). An alternative explanation would consider banding as the periodical shift between tiers of cells possessing a different wall structure (Nash et al., 2019).

In general, the calcifying process of CCA has been described as the deposition of tangential calcite needles in the outer part of the cell wall (interstitial matrix), followed by the formation of radial needles in the cell wall itself in contact with the plasmalemma. The polysaccharide and fibrillary matrix control both processes (Giraud and Cabioch, 1976; Irvine and Chamberlain, 1994; Adey, 1998; de Carvalho et al., 2017). In *L. corallioides*, calcification has been described as being composed of tangential rod-shaped crystals in the primary wall (PW) and perpendicular fan-like rods in the secondary wall (SW) (Giraud and Cabioch, 1976). Borowitzka (1984, 1989) proposed that coralline algae have semi-organized calcification, suggesting that their calcification is biologically controlled, as also indicated by Cabioch and Giraud (1986), rather than induced, as more recently supported by de Carvalho et al. (2017) and Nash et al. (2019). Cell wall ultrastructures are recognized as a valuable tool to define the phenotypic expression of genotypic information (Auer and Piller, 2020). The compelling evidence of a biological con-

trol over calcification in coralline algae was provided by the identification of family-specific cell wall ultrastructures. Epithallial cells in the genus *Lithothamnion* show crystal units as thin rectangular blocks (Auer and Piller, 2020). Seasonality, including seawater temperature oscillations and photoperiod, is considered one of the main factors affecting the growth rate and the biomineralization process (Steller et al., 2007; Kamenos and Law, 2010; Vásquez-Elizondo and Enríquez, 2017), which may influence the ultrastructural pattern.

The identification of CCA in present-day integrative taxonomy is based on genetic methods coupling with the morphological description and measurement of diagnostic features (for example: Basso et al., 2015; Caragnano et al., 2018; Costa et al., 2019). Species identification in the fossil record is, on the contrary, merely based on the preservation of morphological taxonomic characters. Consequently, the identification of valuable morphological characters as a tool for the definition of the paleontological species represents an important challenge. CCA are well represented in the fossil record, and *L. corallioides* has been reported in the Pliocene of Spain (Aguirre et al., 2012) and in the Pleistocene of southern Italy (Bracchi et al., 2014).

This study is aimed at describing the ultrastructural mineralogical features of *L. corallioides* from different geographic settings (northeastern Atlantic Ocean and Mediterranean Sea) and across a wide bathymetric interval (12–66 m) to test if the ultrastructural pattern is preserved under different environmental conditions and therefore can be considered as an evident sign of a biologically controlled mineralization. Moreover, the identification of a specific ultrastructural pattern could be considered as a valuable tool for species identification to be used also in paleobiology. *L. corallioides* has been targeted because of its wide distribution, both geographically and bathymetrically, and its occurrence in the fossil record.

## 2 Materials and methods

For this study, we considered five collections (Fig. 1, Table 1) from two different geographic settings, the Atlantic Ocean and the western Mediterranean Sea, sampled by scuba diving or grabbing at different depths ranging from 12 m in Morlaix Bay (France) down to 66 m in the Pontine Islands (Italy). All specimens have been collected alive. Table 1 reports locations and dates of sampling.

To highlight possible ultrastructural differences among the same genus, two additional collections, already identified as *Lithothamnion minervae* Basso, 1995, and *Lithothamnion valens* Foslie, 1909, have been considered. These collections have been sampled alive from the Egadi Islands (Italy), during July 2016, at 103 and 86 m water depth respectively.

All samples have been air dried and sheltered from sunlight. Once dried, they were stored in plastic boxes with sil-

**Table 1.** Location, date of collection and depth of *L. corallioides* samples. In the “basin” column, numbers in brackets correspond to the point in Fig. 1.

Basin	Sample	Location	Date of collection	Depth (m)	No. of branches	Temperature seasonal range (°C)
Atlantic Ocean (1)	France, Morlaix Bay	48°34′42″ N 3°49′36″ W	May 1991	12	23	8.3–17.2
Western Mediterranean (2)	Italy, Egadi Islands	37°58′10″ N 12°03′26″ E	Aug 1991	40	20	13.7–18.8
Western Mediterranean (3)	Italy, Santa Caterina shoal	39°08′32″ N 9°31′14″ E	Jul 2017	40	12	13.2–20
Western Mediterranean (4)	Italy, Elba island	42°44′56.4″ N 10°07′08.4″ E	Dec 1990	45	20	12.9–17.5
Western Mediterranean (5)	Italy, Pontine Islands	40°54′ N 12°45′ E	Jul 2016	66	12	13.9–16.7

ica to avoid any decay and transported to the laboratories of the University of Milano-Bicocca.

The seawater temperature has been extracted from 11 years of monthly reanalysis spanning 1979–2017 from ORAS5 (Ocean Reanalysis System 5), at 0.25° horizontal resolution (Zuo et al., 2019), to indicate the seasonal temperature fluctuation (Table 1).

## 2.1 Coralline sample preparation

Samples have been prepared for scanning electron microscope (SEM) imaging. Altered, badly preserved or encrusted branches have been discarded. Only the branches showing a shiny surface have been picked from all collections, each controlled under a stereo microscope, and cleaned manually by removing epiphytes and other encrustations. Each sample, composed of multiple branches, has been cleaned in an ultrasonic bath in distilled water for 10 min and air-dried. The branches were then placed in small cylindrical plastic boxes with a base diameter of 1″ (2.54 cm). Branches have been piled up and aligned to obtain multiple layers. The samples were embedded in Epofix resin for SEM analyses, which was stirred for 2 min with a hardener (13 % *w/w*), and they were left to harden for 1 d at room temperature. Samples have then been cut normal to the multiple layers by using an IsoMet diamond wafering blade 15HC, along the direction of branch growth. The number of branches per sample are indicated in Table 1. Moreover, two additional samples (*L. minervae* and *L. valens*) have been prepared for SEM observations ( $n = 10$  branches) by breaking them with a small chisel. Both longitudinal and surface sections have been selected for SEM observations.

## 2.2 Scanning electron microscope

For SEM imaging, the surfaces of embedded samples have been polished by using different sizes of silicon carbide, cleaned ultrasonically in distilled water for 10 min and air-dried. Samples mounted directly on stub have been simply chrome-coated. SEM images have been taken with a field emission gun scanning electron microscope (SEM-FEG): Zeiss Gemini 500 and a TESCAN VEGA TS 5136XM. Standard magnifications for SEM images were established ( $\sim 2500\times$ ,  $\sim 5000\times$ ,  $\sim 10000\times$ ,  $\sim 20000\times$  and  $\sim 30000\times$ ) to describe comparatively and measure growth bands and cells, the morphology of Mg-calcite crystals, and the main features of perithallial and epithallial cell walls. A rigorous control over cell orientation is required to represent, describe and measure in 2D the main features of a 3D structure such as cell calcification (both PW and SW). Longitudinal axial sections of branches are a standard representation for calcareous red algae, allowing for subsequent visual comparison (Woelkerling, 1988; Quaranta et al., 2007; Burdett et al., 2011). Surface tangential sections are useful to describe the epithallial cells. Transverse or oblique sections are useful to describe qualitatively the 3D aspects and organization of calcite crystals composing both PW and SW. Description of the cell wall structure follows the nomenclature of Flajs (1977), presenting the PW and SW calcifications of the wall. Some authors refer to PW as interstitial calcite (Ragazzola et al., 2016) or interfilament calcite (Nash and Adey, 2017; Nash et al., 2013, 2015). Cell dimensions have been measured as reported in Fig. 2 ( $n = 10$  per sample) exclusively on longitudinal sections (Fig. 2). Separation among adjacent filaments was not always obvious (Fig. 2c). In such cases, the PW of adjacent cells has been measured in total (green line in Fig. 2c), and then half of the total was attributed to each cell. In the text we use the term *ultrastructure* to identify the

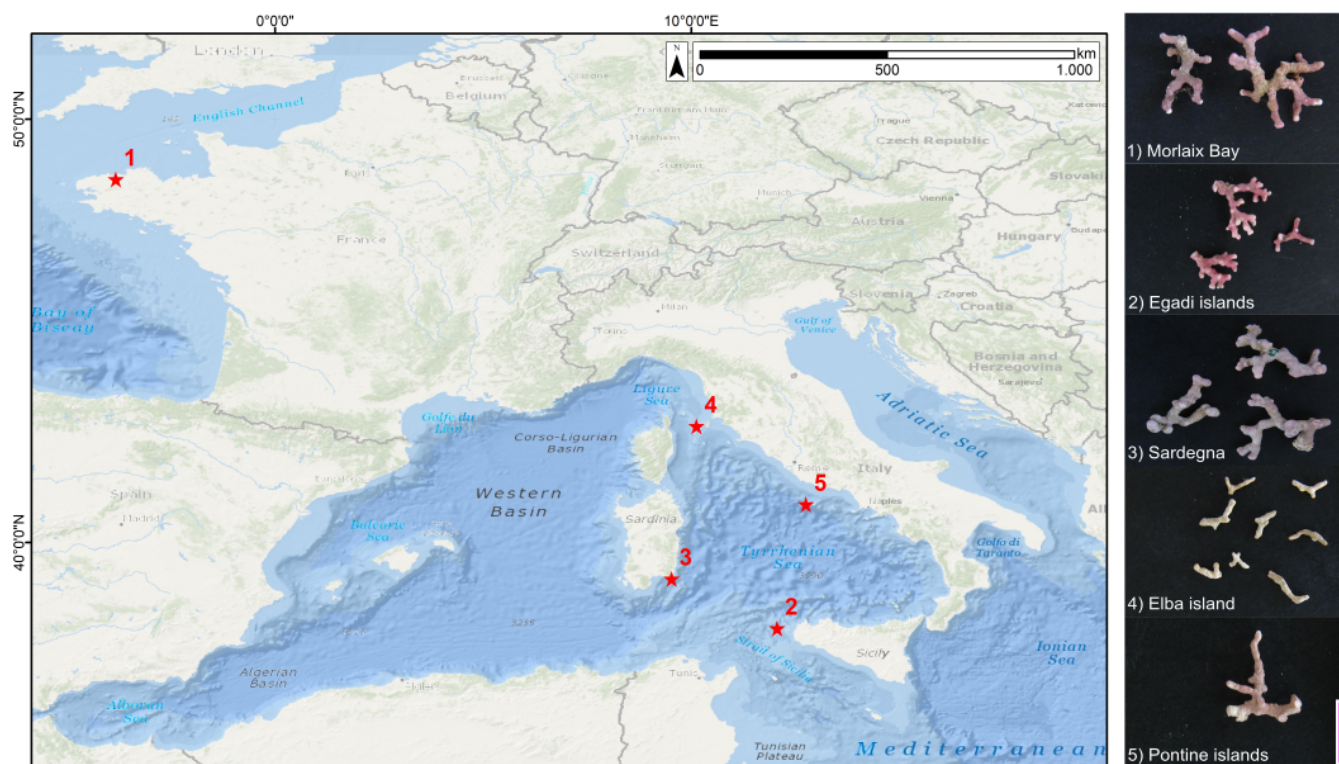


**Figure 1.** Sampling sites (1–5) and images of selected samples. Service layer credit sources: Esri, GEBCO, NOAA, National Geographic, Garmin, HERE, Geonames.org and other contributors. Scale bar = 1 cm.

singular crystal in one of the layers of the cell wall and *ultrastructural pattern* to indicate the combination and mutual organization of crystals in layers of the cell wall.

### 2.3 Statistical analyses

Spearman and Pearson correlations were used to test the statistical relationship between the cell measurements in both long and short cells, including morphometry and cell wall thickness. The linear correlation between the mean cell lengths and the sampling depths was measured by Pearson's coefficient as well. One-way ANOVA and the Kruskal–Wallis tests respectively followed by the Tukey's test and the Dunn's test for post hoc analysis were used to compare the cell measurements among sampling sites and to provide evidence of the differences between group means and medians. All statistical analyses were run in R 3.6.3 software.

### 2.4 Growth rates

Growth rates were estimated under light microscope by measuring a linear transect on the longitudinal section and counting the number of growth bands of fourth order (sensu Foster, 2001) crossed by the transect. The growth rate has been calculated by dividing the length of the transect by the number of growth bands.

## 3 Results

### 3.1 Ultrastructures from SEM images

Selected rhodoliths belong to the unattached branches morphotype (Basso, 1998; Basso et al., 2016), never exceeding 3 cm in length (Fig. 1). The diameter of each branch never exceeds 2.5 mm (Fig. 1). The color varies from yellowish white to pink/purplish, with typical knob-like apices (Fig. 1).

Once cut, all samples show the same micromorphology (Fig. 3a–i, Supplement 2), with the constant occurrence of an easily detectable banding due to the alternation of series of short and long cells (Fig. 3a, b) in bands of the fourth order corresponding to 1 year (Foster, 2001). No reproductive structure (conceptacle) was detected.

Along the perithallus, long cells are ovoid to rectangular in shape (Fig. 3c, d, Supplement 2), whereas short cells are more squared (Fig. 3e, f).

Within the long-celled bands, the longest cells were measured in the sample from Morlaix Bay ( $26.71 \pm 1.74 \mu\text{m}$ ), while the less elongated cells were observed in the sample from the Pontine Islands ( $13.05 \pm 0.76 \mu\text{m}$ ) (Table 2, Fig. 4).

Within the short-celled bands, the shortest cells were observed in the sample from Pontine ( $6.97 \pm 0.25 \mu\text{m}$ ), while the longest short cells were from Morlaix Bay ( $13.90 \pm 0.88 \mu\text{m}$ ) (Table 2, Fig. 4). Cell diameter ranges

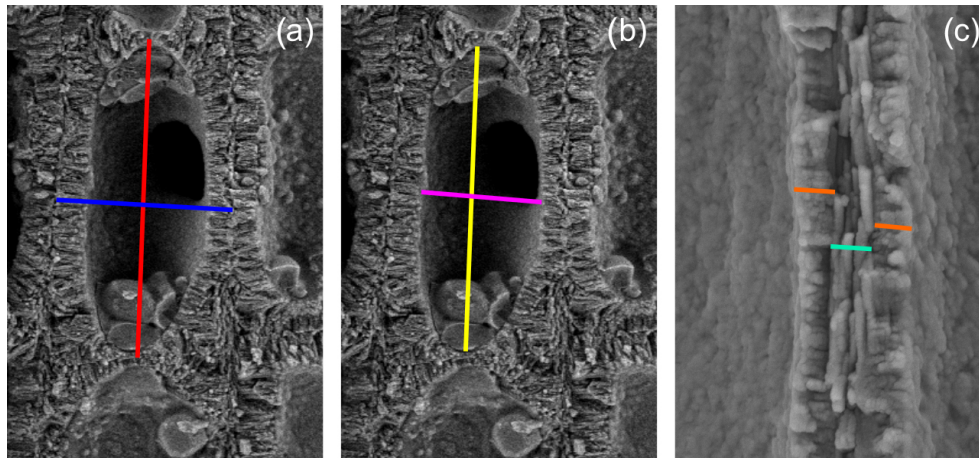


**Figure 2.** Cell measurements: (a) cell wall length (red) and diameter (blue); (b) lumen length (yellow) and lumen diameter (purple); (c) SW thickness of adjacent cells (orange); PW thickness of adjacent cells (green).

**Table 2.** Morphometry of short and long cells and lumens and wall thickness measured in longitudinal section (PW = primary wall, SW = secondary wall) with the indication of length (L) and diameter (D) ( $\mu\text{m}$ ). Standard deviation in brackets.

Sample	Short cell						Long cell					
	Cell		Lumen		Wall		Cell		Lumen		Wall	
	L	D	L	D	SW	PW	L	D	L	D	SW	PW
Morlaix Bay 12 m	13.90 (0.88)	8.31 (1.34)	12.38 (0.93)	6.04 (1.05)	1.61 (0.43)	0.12 (0.03)	26.70 (1.73)	11.11 (1.80)	24.46 (1.73)	9.25 (1.42)	0.57 (0.14)	0.13 (0.06)
Egadi Islands 40 m	13.43 (2.36)	9.22 (0.70)	8.48 (1.189)	4.97 (1.55)	2.08 (0.80)	0.22 (0.07)	18.55 (1.28)	10.27 (0.77)	16.13 (1.16)	8.54 (0.60)	0.74 (0.09)	0.16 (0.05)
Santa Caterina shoal 40 m	10.57 (1.01)	8.29 (0.58)	8.79 (0.72)	4.43 (0.66)	1.87 (0.26)	0.17 (0.16)	16.80 (1.54)	7.69 (1.07)	15.40 (1.51)	5.04 (0.81)	1.25 (0.41)	0.13 (0.03)
Elba island 45 m	12.8 (0.45)	9.4 (0.9)	11.6 (0.54)	5.2 (0.44)	2.2 (0.44)	0.14 (0.05)	17.51 (0.78)	8.64 (0.81)	15.75 (0.89)	6.31 (0.83)	1.08 (0.25)	0.18 (0.06)

between  $7.69 \pm 1.07 \mu\text{m}$  (Santa Caterina shoal) and  $11.11 \pm 1.79 \mu\text{m}$  (Morlaix) in long cells and between  $8.27 \pm 0.48 \mu\text{m}$  (Pontine) and  $9.23 \pm 0.70 \mu\text{m}$  (Egadi) in short cells (Table 2, Fig. 4).

Both long and short cells have PWs and SWs, and the style of mineralization shows a consistent ultrastructural pattern. The PW crystallization observed in longitudinal medial sections (cutting the cell lumen) is composed of elongated crystals appearing as rods (Fig. 5a–c, e), but where longitudinal sections are tangential to the PW, crystals are revealed to be flat rectangular tiles (Figs. 5d, f, 6a). The long axis of the PW tiles is parallel to the cell membrane and may form a multi-layered structure which envelops the cell (Fig. 5e). The dimensions of the tiles are  $0.61 \pm 0.17 \mu\text{m}$  in length and  $0.05 \pm 0.01 \mu\text{m}$  in height (Fig. 6a). Elongated radial crystals (Fig. 7a, b) in longitudinal sections cutting the cell lumen characterize the SW. Small, roundish units, appearing as being fused together, in places showing an ap-

parent multi-layered structure (Fig. 7b) form such crystals. These elongated crystals are radial to the cell lumen (Fig. 7a–c). Where the cell membrane is lost, the SW can be observed from different orientations, and such apparently elongated crystals are revealed to be thin bricks with rounded margins (Figs. 6b, 7d–f). Bricks are squared, and length and width are  $0.63 \pm 0.15 \mu\text{m}$  (Fig. 6b). The bricks form a sort of envelope around the cell (Figs. 6b, 7e, f), showing sometimes a zigzag and cross orientation (Fig. 7g, h).

Different thicknesses characterize the PW and SW of short and long cells (Figs. 3, 5, 7; Table 2, Supplement 2) in longitudinal medial sections. Both PW and SW of short cells are generally thicker than in long cells (Table 2) even if the thickness does not show a correlation with sampling bathymetry. The SW thickness ranges between  $1.52 \pm 0.65 \mu\text{m}$  (Pontine) and  $2.20 \pm 0.45 \mu\text{m}$  (Elba) in short cells and between  $0.57 \pm 0.14 \mu\text{m}$  (Morlaix) and  $1.26 \pm 0.42 \mu\text{m}$  (Santa Caterina shoal) in long cells (Table 2).

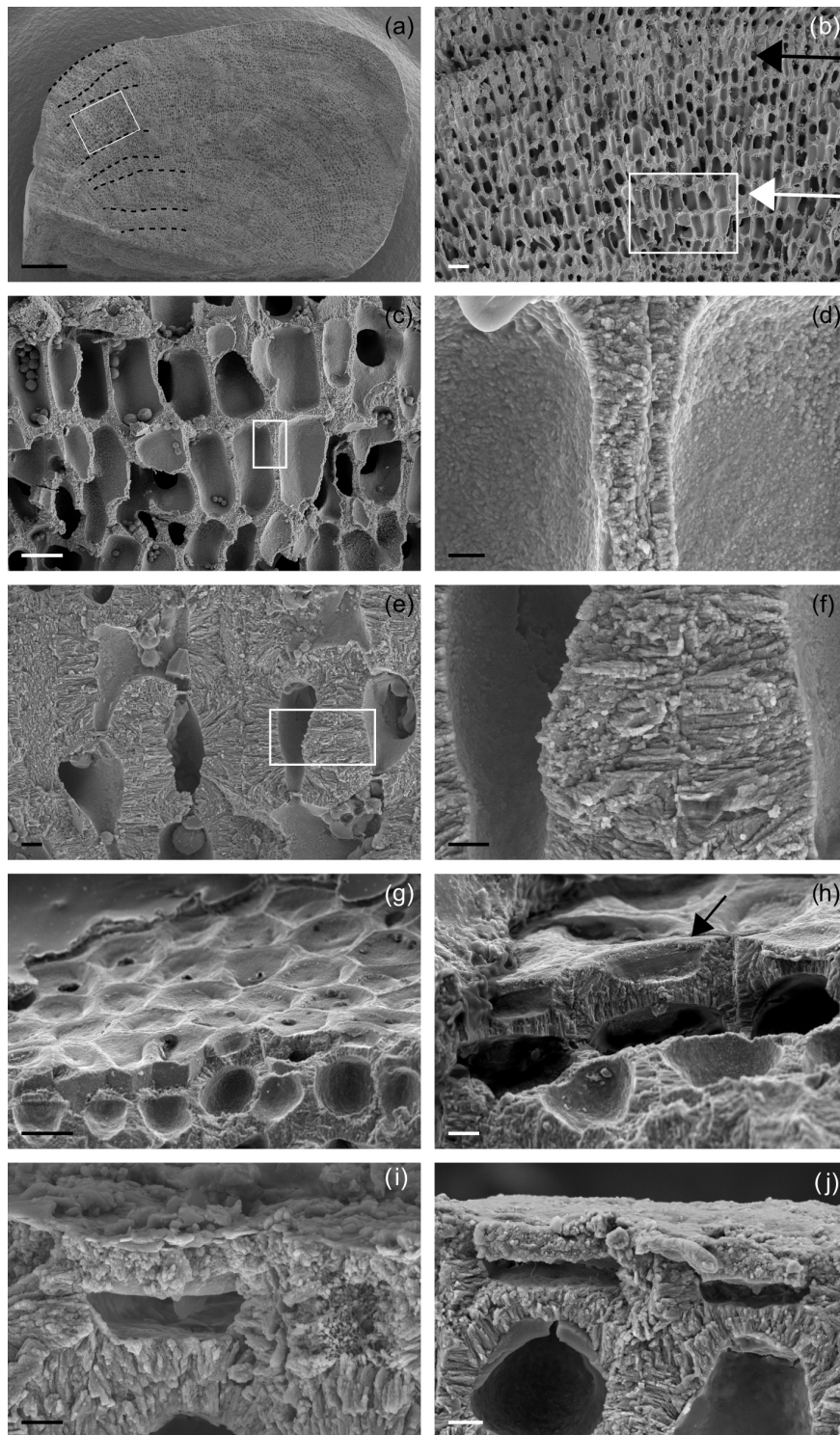


**Figure 3.** Main features of *Lithothamnion corallioides* under SEM (Morlaix Bay, France). **(a)** Longitudinal section of *L. corallioides* with obvious banding (dashed black lines). Scale bar = 100  $\mu\text{m}$ . The inset is magnified in **(b)**; **(b)** alternation of thick-walled (black arrow) and thin-walled (white arrow) cells. Scale bar = 20  $\mu\text{m}$ . The inset is magnified in **(c)**; **(c)** thin-walled long cells. Scale bar = 10  $\mu\text{m}$ . The inset is magnified in **(d)**; **(d)** detail of the thin wall of long cells. Scale bar = 1  $\mu\text{m}$ . **(e)** Thick-walled short cells. Scale bar = 2  $\mu\text{m}$ . The inset is magnified in **(f)**; **(f)** detail of the thick wall of short cells. Scale bar = 1  $\mu\text{m}$ . **(g)** Polygonal shape of epithallial cells in surface view. Scale bar = 10  $\mu\text{m}$ . **(h)** Detail of a flared epithallial cell (arrow). Scale bar = 3  $\mu\text{m}$ . **(i–j)** Longitudinal sections of flared epithallial cells with complete mineralization of the cell walls. Scale bar = 2  $\mu\text{m}$ .

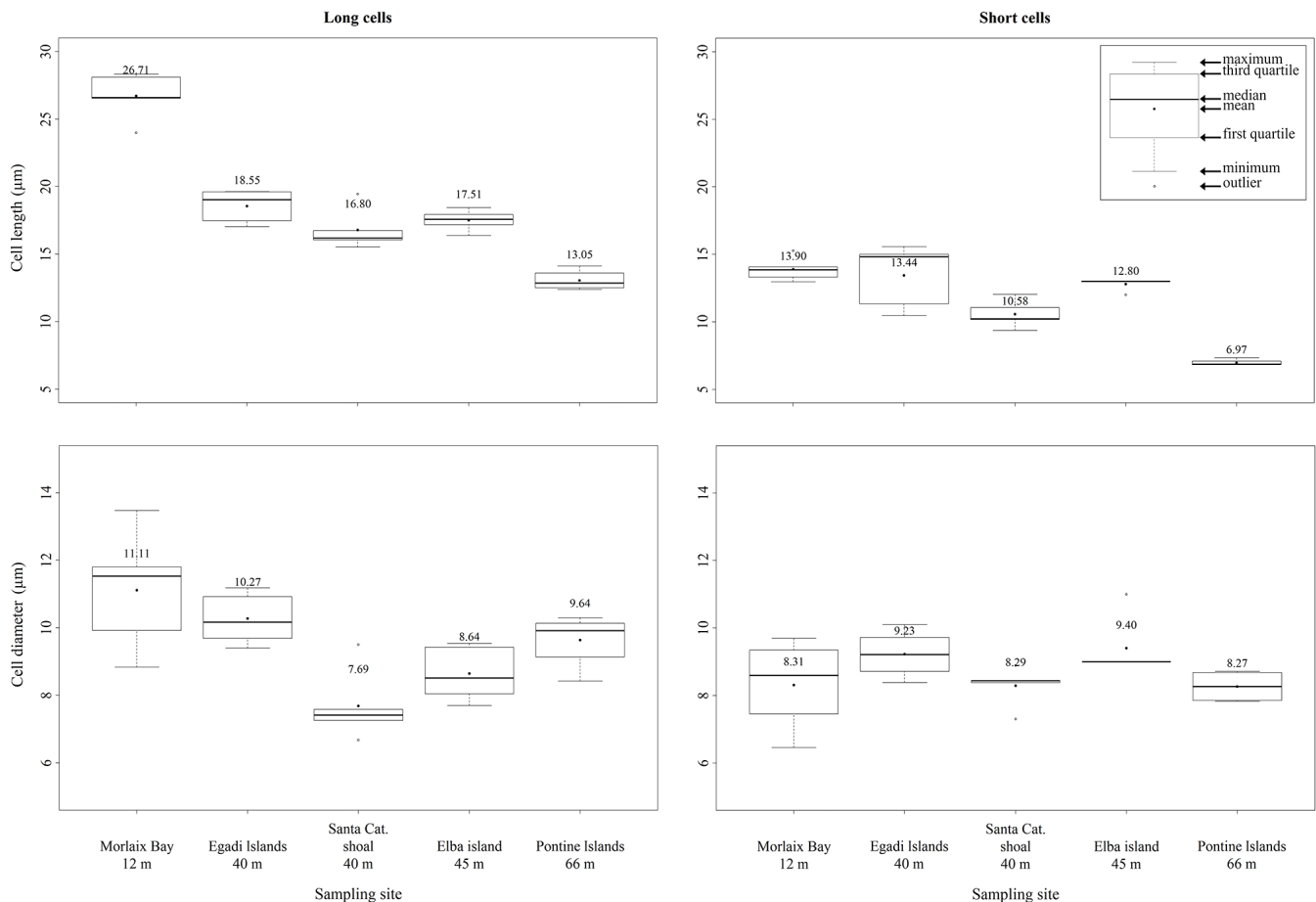


**Figure 4.** Box plots reporting cell lengths and cell diameters in both long and short cells of *L. corallioides* collected at different sampling sites and ordered along  $x$  axis according to the depth.

Both PW and SW show fibrils (Borowitzka, 1982) forming a dense network in support of the mineralization (Fig. 7d).

The epithallus is formed by one to three flared cells in longitudinal sections (Figs. 3g–j, 5f, 7c), always mineralized, with some exceptions in the top distal surface (Fig. 3g–j). The cell wall shows the same ultrastructural features of the perithallial cells, with both PW and SW mineralized (Figs. 3i, j, 5f, 7c).

Based on image analysis and time of collection, the calculated growth rate ranges from 0.10 mm/yr in Pontine to 0.13 mm/yr in both Morlaix and Egadi.

The two additional collections of *L. valens* and *L. minervae* (Fig. 8) are characterized by both PW and SW (Fig. 8a, b, e, f). The SW shows, in both species, an ultrastructural pattern like the one described for *L. corallioides*, with oriented bricks with rounded margins variably orientated, only apparently elongated and radial to the cell lumen in longitudinal sections (Fig. 8b, f). If observed in the cell lumen, where the cell membrane is lost, the SW shows bricks with different orientation and sometimes a zigzag and cross orientation (Fig. 8d, g).

On the contrary, PW shows a different shape and arrangement of crystals which are not characterized by the tiles of *L. corallioides* observed in Figs. 5d and 6a. Calcite crystals are squatter and more granular (Fig. 8a) or with irregular shape (Fig. 8h). One interesting aspect is that both samples show the occurrence of secondary calcite in the form of dogtooth crystals filling the cell lumen (Fig. 8b, c, e).

### 3.2 Statistical analyses on morphological parameters

The differences in the long cells' morphometry and wall thickness among sampling sites are statistically significant for each measured parameter ( $p < 0.05$ ; Supplement 1) (Fig. 9). Interestingly, the long-cell length of the deepest sample from Pontine Islands (66 m depth) is lower than the others ( $p < 0.001$ ) (Figs. 4, 9; Supplement), while in the shallowest sample collected in Morlaix (12 m depth) cells are remarkably longer ( $p < 0.001$ ) (Figs. 4, 9; Supplement 1).

In short cells, significant differences result only for cell (Fig. 9) and lumen lengths, as well as cell PW ( $p < 0.05$ ; Supplement). The shortest cells are observed again in the sam-

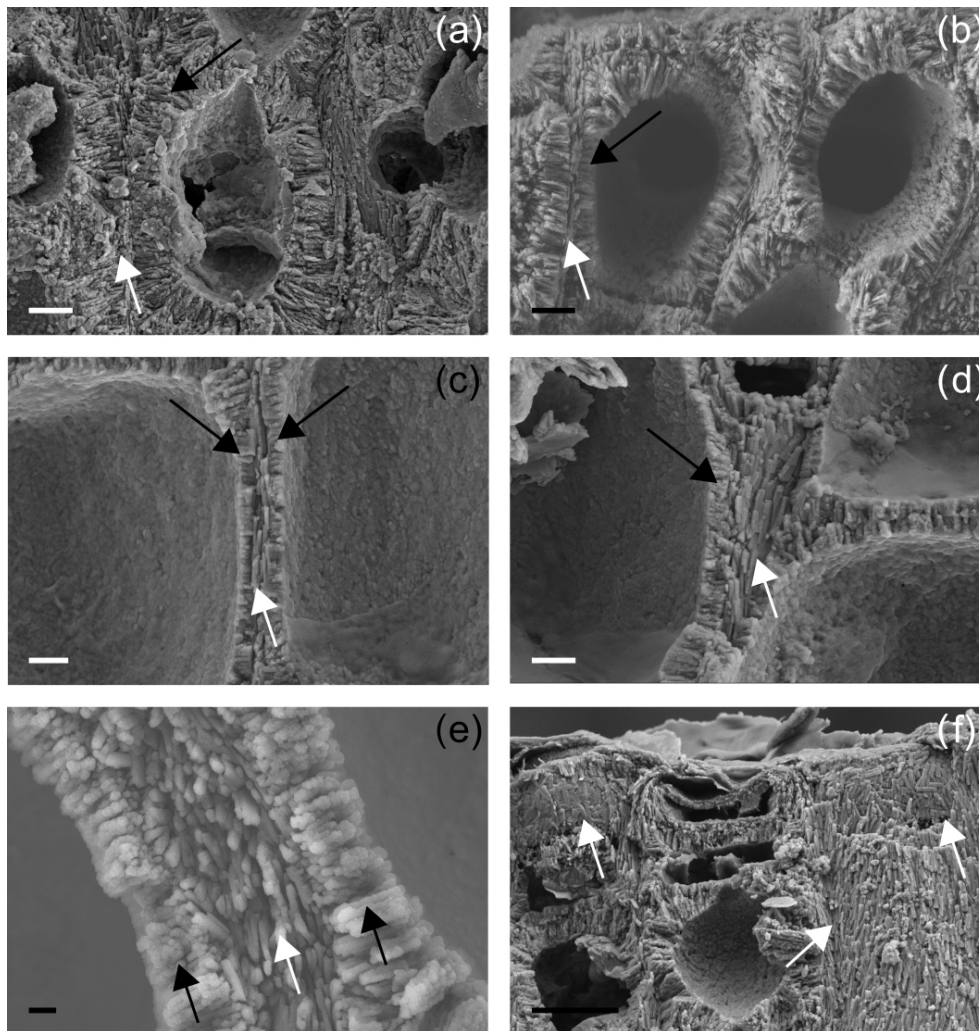


**Figure 5.** Details on primary wall (PW) in longitudinal section. (a) Thick-walled short cell showing both PW (white arrow) and SW (black arrow) for Santa Caterina shoal. Scale bar = 2  $\mu\text{m}$ . (b) Thick-walled short cell showing both PW (white arrow) and SW (black arrow) for Pontine Islands. Scale bar = 2  $\mu\text{m}$ . (c) Thin-walled long cell showing both PW (white arrow) and SW (black arrows). PW crystals in longitudinal section appear with elongated shape for Santa Caterina shoal. Scale bar = 1  $\mu\text{m}$ . (d) Thin-walled long cell showing both PW (white arrow) and SW (black arrow). The fracture shows detail of tiles composing the PW (white arrow) and SW (black arrows) for Santa Caterina shoal. Scale bar = 1  $\mu\text{m}$ . (e) Details of multi-layered PW (white arrow) and SW (black arrows). PW crystals in longitudinal section appear as elongated crystals for Pontine Islands. Scale bar = 0.2  $\mu\text{m}$ . (f) Perithallial and epithallial cells in which the longitudinal section is locally tangential to the PW (white arrows). Crystals appear as flat rectangular tiles for Santa Caterina shoal. Scale bar = 2  $\mu\text{m}$ .

ple from Pontine Islands, differing from the one collected in Morlaix ( $p < 0.01$ ) (Fig. 9; Supplement 1), which stands out for being the highest value. On the contrary, the cell diameter slightly varies among sites, showing significant differences just in long cells ( $p < 0.01$ ; Supplement 1) (Fig. 9), with significantly higher values in Morlaix with respect to Elba island and Santa Caterina. The dimensions of the cell lumen change accordingly because of the positive correlation with the cell dimensions (Supplement 1).

Although banding is reported for all samples, elongation decreases with increasing depth, showing a strong inverse correlation in long cells ( $p < 0.01$ ;  $r = 0.98$ ) (Fig. 9). The

same trend is also observed in short cells, although with non-significant values ( $p = 0.09$ ) (Fig. 9).

#### 4 Discussion

Properly oriented longitudinal and transverse/oblique sections are required to obtain a precise comparative description of the main morphological features of CCA. Multi-scale approaches are also relevant, among which the ultrastructural pattern may represent a new powerful and strategic diagnostic tool (Figs. 3–7).



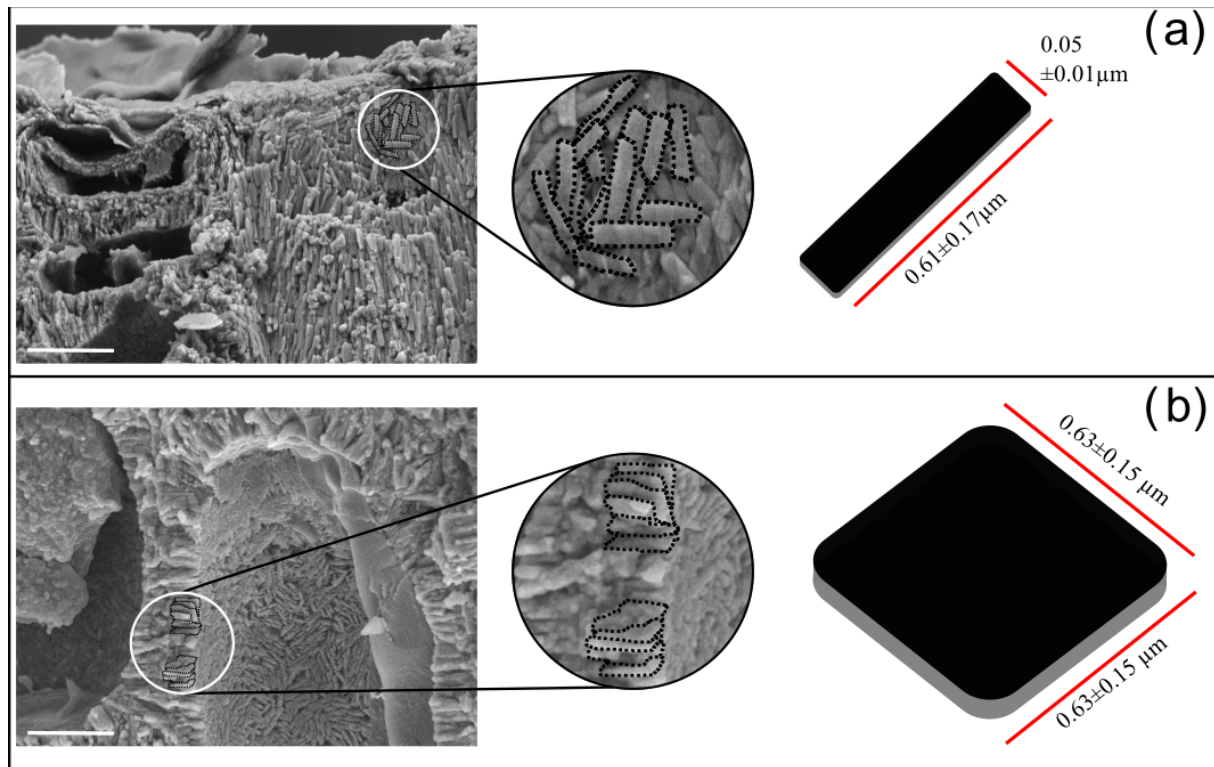


**Figure 6.** Ultrastructures of *Lithothamnion corallioides*: (a) rectangular tiles of the PW; (b) squared bricks of SW.

Recent studies based on genetic identification exclude the occurrence of other *Lithothamnion* species in the maerl of Morlaix Bay (Carro et al. 2014; Melbourne et al., 2017). Based on this identification and considering the macroscopic features, the thallus pattern, the microanatomy, the morphology and the morphometry of cell walls (Figs. 3, 5–7, Table 2), we identified the samples from Morlaix Bay as belonging to the species *L. corallioides*.

We compared the Mediterranean specimens with the Atlantic *L. corallioides*, and upon corresponding morphology, anatomy and ultrastructure (Figs. 3, 5–7, Table 2), we considered them as conspecific.

The perithallus of *L. corallioides* clearly shows the alternation of growth bands of third and fourth orders (Fig. 3a, b), in agreement with Foster (2001). Fourth-order bands represent the annual cycling, whereas third-order ones represent seasonal variations and can be firstly distinguished by an evident chromatic change due to the different calcification thickness between long and short cells (Foster, 2001). In our samples, the banding (third and fourth orders) is easily recognizable (Fig. 3), and both long and short cell lengths decrease across depths (Figs. 4, 9), as expected, mirroring a decrease in growth rate, whereas the diameter variation is significantly lower (Fig. 4, Supplement 1).

Giraud and Cabioch (1979) observed that a cell wall fracture in *L. corallioides* shows a layer of radial calcite crystals (SW) separated from its neighbor by a different sheet com-

posed of tangential crystals (PW). A discontinuity that coincides with the fibrillar matrix observed in sections of decalcified material marks the limits of adjacent cellular filaments (Giraud and Cabioch, 1979). Our results match with the observations of these authors in longitudinal sections (Figs. 3, 5, 7), although the discontinuity between adjacent cells is not easily detectable because of the complete mineralization.

Auer and Piller (2020) built a morphological tree based on the observation of different ultrastructural patterns in epithelial cells, which matches with the phylogenetic tree at family level. For Hapalidiaceae, and in the *Lithothamnion*-type epithelial ultrastructure, they observed the occurrence of PWs with primary crystals formed along the middle lamella and the SWs with secondary rod-shaped crystals, also presenting fan-like structures. The samples studied in the present work show the PW and SW in both perithallial and epithelial cell walls (Figs. 3, 5, 7). Both are apparently composed of rod-like crystals in longitudinal sections. However, in longitudinal sections that are locally tangential to the PW, the apparent rods are revealed to be the longest and thinnest side of variably oriented rectangular tiles (Figs. 5, 6a). The tiles that envelop the cell (Fig. 5d, f) are the basic ultrastructural elements forming the PW. Differently, apparent rods of the SW are revealed to be squared and relatively flat bricks with rounded margins, as observed at the cell lumen without membrane or exactly at the contact between the SW longitudinal section and cell lumen (Figs. 6b, 7). Crystals in longitudinal

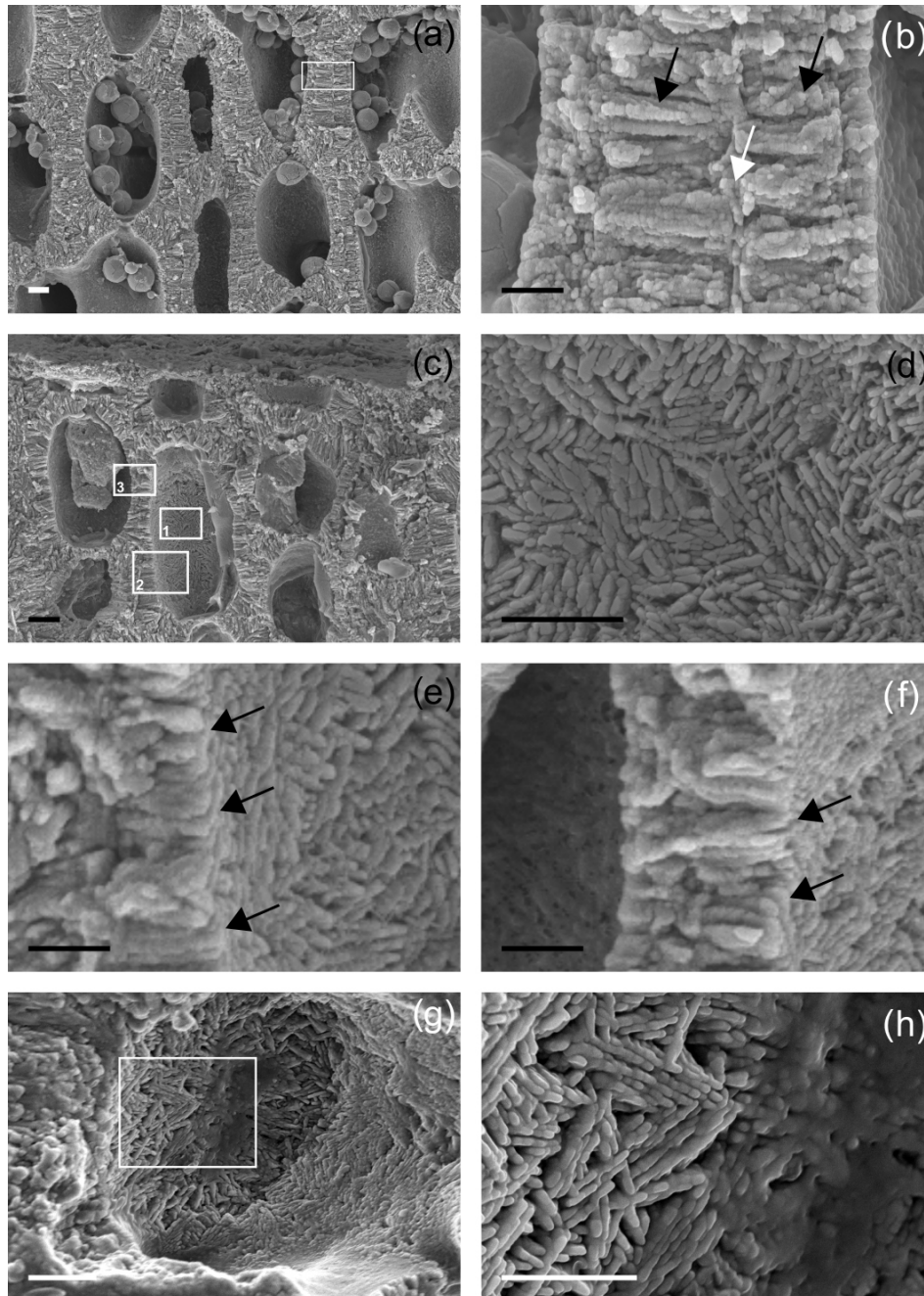


**Figure 7.** Details of secondary wall (SW) in longitudinal section. (a) Thick-walled short cells showing both PW and SW for Morlaix Bay. Scale bar = 2  $\mu\text{m}$ . The inset is magnified in (b); (b) very thin PW (white arrow) and SW (black arrows) in cell walls of two adjacent cells. The SW is characterized by elongated radial crystals formed by the fusion of smaller roundish units, in places showing an apparent multi-layered structure, for Morlaix Bay. Scale bar = 1  $\mu\text{m}$ . (c) Perithallial thick-walled cells showing both PW and SW, as well as single flattened epithallial cells, for Morlaix Bay. Inset 1 is magnified in (d), inset 2 in (e) and inset 3 in (f). Scale bar = 2  $\mu\text{m}$ . (d) The SW as visible in lumen cell with no membrane. In this view the crystals appear to be ovoidal to rod-shaped with a complex orientation associated with fibrils for Morlaix Bay. Scale bar = 1  $\mu\text{m}$ . (e) The SW as visible in lumen cell with no membrane. A section showing at the same time a longitudinal section of the cell wall (on the left) and the inner surface of the lumen cell (on the right). This perspective provides the actual 3D shape of the SW crystals that are thin bricks (black arrows) for Morlaix Bay. Scale bar = 1  $\mu\text{m}$ . (f) The SW as visible in lumen cell with no membrane. A section showing at the same time a longitudinal section of the cell wall (center) and the inner surface of the lumen cell (on the right). This perspective provides the actual 3D shape of the SW crystals that are thin bricks (black arrows) for Morlaix Bay. Scale bar = 1  $\mu\text{m}$ . (g) A detail of the SW as visible inside a cell lumen. The crystals are thin bricks with a complex zigzag and cross orientation. The inset is magnified in (h) for Egadi Islands. Scale bar = 2  $\mu\text{m}$ . (h) A zigzag and cross orientation of bricks in the SW for Egadi Islands. Scale bar = 1  $\mu\text{m}$ .

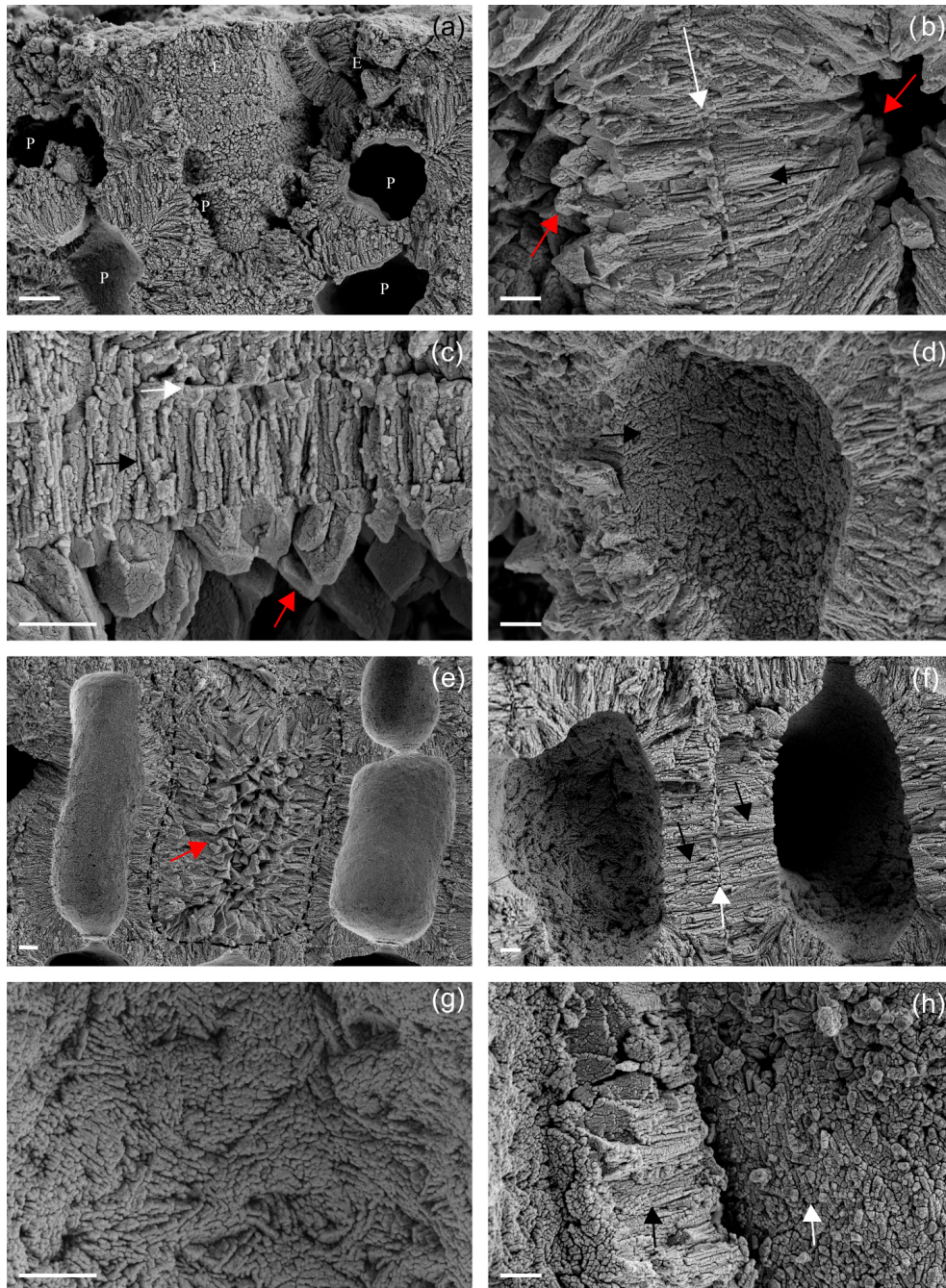


**Figure 8.** Details of the main ultrastructures of *Lithothamnion valens* (a–d) and *Lithothamnion minervae* (e–h). (a) Perithallial (P) and epithallial (E) cells showing both PW and SW. Scale bar = 2  $\mu\text{m}$ . (b) Details of PW (white arrow) and SW (black arrow) of two adjacent perithallial cells. The secondary wall is characterized by elongated radial crystals, whereas PW crystals are tangential to the cell lumen. The cell lumen is filled by secondary calcite (dogtooth shape, red arrows). Scale bar = 1  $\mu\text{m}$ . (c) Detail of a cell wall with evident PW (white arrow) and SW (black arrow), as well as secondary dogtooth calcite filling the cell lumen (red arrow). Scale bar = 2  $\mu\text{m}$ . (d) Detail of SW (black arrow) as visible in the cell lumen with no membrane. Note the multi-directional arrangement of calcite crystals. Scale bar = 2  $\mu\text{m}$ . (e) Perithallial cells with elongated and rectangular shape. The central cell (dashed) shows a cell lumen filled by secondary calcite with dogtooth shape (red arrow). Scale bar = 2  $\mu\text{m}$ . (f) Perithallial cells with both PW (white arrow) and SW (black arrows). Note in the cell lumen that the SW is characterized by elongated crystals showing a multi-directional arrangement. Scale bar = 2  $\mu\text{m}$ . (g) Detail of the cell lumen with no membrane, showing multi-directional arrangement of elongated crystals in the SW. Scale bar = 1  $\mu\text{m}$ . (h) The fracture shows detail of crystals composing the PW (white arrow) apparently composed of granules. The SW is characterized by elongated crystals in longitudinal section (black arrow). Scale bar = 1  $\mu\text{m}$ .

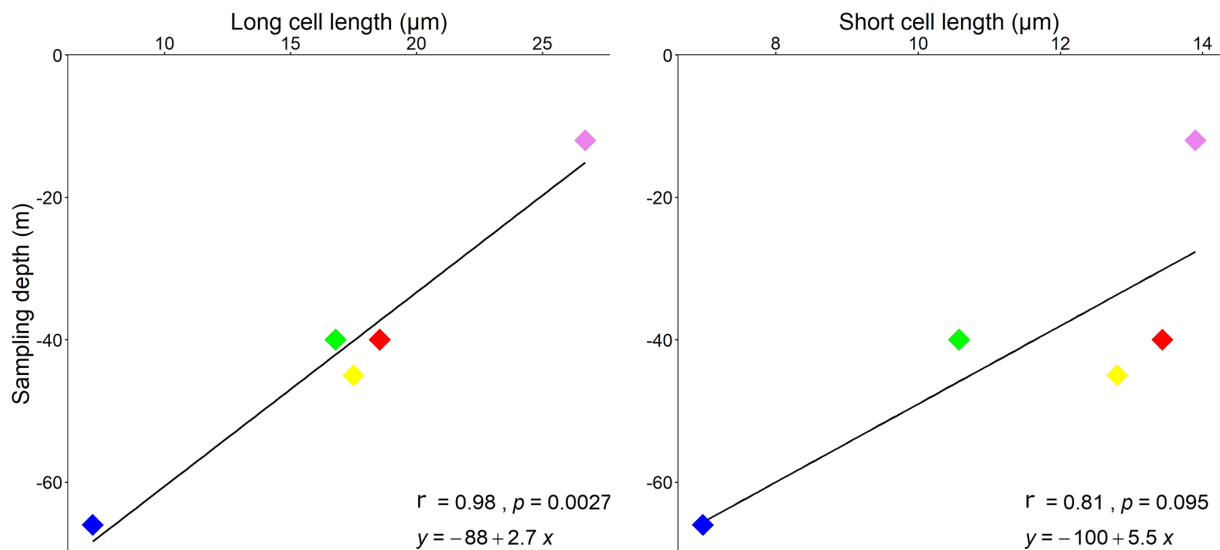


**Figure 9.** Correlation plots showing the relationship between sampling depth and cell lengths, measured in both long and short cells. Pearson's correlation significance at  $p < 0.05$ . Pink is for Morlaix Bay (France, 12); green is for Egadi Islands (Italy, 40); red is for Santa Caterina shoal (Italy, 40); yellow is for Elba island (Italy, 45); blue is for Pontine Islands (Italy, 66).

sections of the SW are radial to the cell lumen, in agreement with Giraud and Cabioch (1979), and appear formed by small grains fused together (Figs. 3, 7b, f). They can also show a zigzag and cross orientation (Fig. 7g, h) like the fan-delta structure described by Auer and Piller (2020).

Therefore, our findings agree with the results of Auer and Piller (2020), although providing a more detailed description of the ultrastructural pattern of *L. corallioides* (Fig. 6).

Despite the different environmental conditions, likely occurring at the different sampling sites and depths, the ultrastructures of both PW and SW seem conservative and detectable in all samples. Therefore, the ultrastructures and the ultrastructural pattern are not dependent on environmental controls.

However, *L. corallioides* shows variable cell elongations (Table 2) and growth rates, both decreasing according to sampling depth (Fig. 9), and a variation in PW and SW thickness, generally greater in short than in long cells, unrelated to depth (Table 2, Supplement 1). These features possibly represent the effect of the different environmental conditions in which it lives that do not affect the ultrastructural pattern.

As defined by Lowenstam (1981), a biologically controlled biomineralization is recognized in organisms with extensive control over their mineral formation, resulting in well-ordered mineral structures with minor size variations and species-specific crystal habits, as we detected in *L. corallioides*. Despite some analogies with the observations of Nash et al. (2019), our findings demonstrate that the biomineralization process in CCA is biologically controlled (Borowitzka, 1984; Cabioch and Giraud, 1986) rather than induced (de Carvalho et al., 2017; Nash et al., 2019). The two additional samples, *L. minervae* and *L. valens*, show dis-

tinct styles of PW calcification, and this is extremely interesting for its application in Paleontology. Ultrastructures and ultrastructural pattern possibly represent a powerful tool for morphological species identification. Further investigation is needed to clarify the validity of this hypothesis in other genera and species.

Finally, the occurrence of calcite in the form of dogtooth crystals filling the cell lumen (Fig. 8b, c, e) is an exceptional finding. The voids of the cell lumens allowed for the development of calcite crystals which in terms of shape, size and pattern are completely different from the original ones forming the cell wall calcification. It represents a form of extremely early alteration, possibly diagenesis, in collections that were alive at the time of sampling. The phenomenon of earliest diagenesis, as already observed in Holocene and live Scleractinia corals (Nothdurft and Webb, 2008; Rashid et al., 2020), has implications in the reliability of climate and paleoclimate studies based on geochemical techniques and also when applied to recent collections. Therefore, the possible occurrence of dog-tooth calcite must be carefully checked when selecting coralline algae samples for geochemical investigations.

## 5 Conclusions

We define the cell wall ultrastructural pattern of *L. corallioides* as follows:

- perithallus with evident banding as the result of the alternation of series of short-squared and long ovoid/rectangular cells;
- epithallus with one to three flared cells;

- same and consistent ultrastructural pattern of the cell walls both in perithallus and epithallus, with PW and SW calcite walls always present;
- PW characterized by rectangular tiles;
- SW characterized by flattened squared bricks with roundish outlines;
- long and short cells with similar diameter and with different thickness of the PW and SW, resulting mainly in a thicker PW and SW in short cells.

The variable cell elongation, decreasing according to depth and producing an evident banding, never affects the ultrastructural pattern that maintains the same arrangement also under different growth rates. These findings demonstrate that the CCA calcification process seems to be biologically controlled rather than induced. The comparison with other *Lithothamnion* species highlights differences in the mineralization pattern of PW. Therefore, the ultrastructure of the cell wall in CCA results in a promising new diagnostic tool for species identification with important potential applications in paleontology. Lastly, an early alteration phenomenon, at the scale of ultrastructures, has been identified for the first time in living coralline algae.

**Data availability.** All data of this study are available in this text and in the Supplement.

**Supplement.** The supplement related to this article is available online at: <https://doi.org/10.5194/bg-18-6061-2021-supplement>.

**Author contributions.** VAB conceived the research, conducted SEM observations, interpreted the results, and wrote and revised the manuscript. DB conceived the research, and wrote and revised the manuscript. GP conducted the statistical analyses and prepared Figs. 4 and 9.

**Competing interests.** The contact author has declared that neither they nor their co-authors have any competing interests.

**Disclaimer.** Publisher's note: Copernicus Publications remains neutral with regard to jurisdictional claims in published maps and institutional affiliations.

**Acknowledgements.** We are grateful to two anonymous reviewers for their fruitful comments on the manuscript. Agostino Meroni is thanked for the extraction of temperature values. For the sample from Pontine Islands, the captain, crew and scientific staff of RV *Minerva Uno* cruise Strategia Marina Ligure-Tirreno are acknowledged for their efficient and skillful cooperation at sea. The sample

from Capo Carbonara has been collected in the framework of the agreement between the University of Milano-Bicocca and the Marine Protected Area of Capo Carbonara for the realization of the monitoring activities of the Marine Strategy Framework Directive.

Giulia Piazza is funded by a doctoral fellowship in Environmental Sciences of the Milano-Bicocca University.

This article is a contribution to the Project MIUR-Dipartimenti di Eccellenza 2018–2022 DISAT-UNIMIB.

**Review statement.** This paper was edited by Hiroshi Kitazato and reviewed by two anonymous referees.

## References

- Adey, W. H.: Coralline algae as indicators of sea-level, in: *Sea-Level Research*, edited by: van de Plassche, O., Springer, Dordrecht, [https://doi.org/10.1007/978-94-009-4215-8\\_9](https://doi.org/10.1007/978-94-009-4215-8_9), 1986.
- Adey, W. H.: Review-coral reefs: algal structured and mediated ecosystems in shallow, turbulent, alkaline waters, *J. Phycol.*, 34, 393–406, <https://doi.org/10.1046/j.1529-8817.1998.340393.x>, 1998.
- Adey, W. H. and McKibbin, D. L.: Studies on the Maerl Species *Phymatolithon calcareum* (Pallas) nov. comb. and *Lithothamnium corallioides* Crouan in the Ria de Vigo, *Bot. Mar.*, 13, 100–106, <https://doi.org/10.1515/botm.1970.13.2.100>, 1970.
- Agnesi, S., Babbini, L., Bressan, G., Cassese, M. L., Mo, G., and Tunesi, L.: Distribuzione della Facies del Maerl e delle associazioni a rodoliti nei mari italiani: attuale stato delle conoscenze, *Biol. Mar. Medit.*, 18, 50–51, 2011.
- Aguirre, J., Riding, R., and Braga, J.: Diversity of coralline red algae: Origination and extinction patterns from the Early Cretaceous to the Pleistocene, *Paleobiology*, 26, 651–667, [https://doi.org/10.1666/0094-8373\(2000\)026<0651:DOCRAO>2.0.CO;2](https://doi.org/10.1666/0094-8373(2000)026<0651:DOCRAO>2.0.CO;2), 2000.
- Aguirre, J., Braga, J. C., Martín J. M., and Betzler C.: Paleoenvironmental and stratigraphic significance of Pliocene rhodolith beds and coralline algal bioconstructions from the Carboneras Basin (SE Spain), in: *Calcareous algae and global change: from identification to quantification*, edited by: Basso, D. and Granier, B., *Geodiversitas*, 34, 115–136, <https://doi.org/10.5252/g2012n1a7>, 2012.
- Auer, G. and Piller, W. E.: Nanocrystals as phenotypic expression of genotypes – An example in coralline red algae, *Sci. Adv.*, 6, eaay2126, <https://doi.org/10.1126/sciadv.aay2126>, 2020.
- Basso, D.: Living calcareous algae by a paleontological approach: the genus *Lithothamnion* Heydrich nom. cons. from the soft bottoms of the Tyrrhenian Sea (Mediterranean), *Riv. It. Pal. Strat.*, 101, 349–366, doi10.13130/2039-4942/8592, 1995.
- Basso, D.: Deep rhodolith distribution in the Pontian Islands, Italy: a model for the paleoecology of a temperate sea, *Palaeogeogr. Palaeoclimatol.*, 137, 173–187, 1998.
- Basso, D., Fravega, P., and Vannucci, G.: The taxonomy of *Lithothamnium ramosissimum* (Gümbel non Reuss) Conti and *Lithothamnium operculatum* (Conti) Conti (Rhodophyta, Corallinaceae), *Facies*, 37, 167–181, <https://doi.org/10.1007/BF02537377>, 1997.

- Basso D., Nalin R., and Massari F.: Genesis and composition of the Pleistocene Coralligène de plateau of the Cutro Terrace (Calabria, southern Italy), *Neues Jahrb. Geol. P.-A.*, 244, 173–182, <https://doi.org/10.1127/0077-7749/2007/0244-0173>, 2007.
- Basso, D., Caragnano, A., Le Gal, L., and Rodondi, G.: The genus *Lithophyllum* in the north-western Indian Ocean, with description of *L. yemenense* sp. nov., *L. socotraense* sp. nov., *L. subplicatum* comb. et stat. nov., and the resumed *L. affine*, *L. kaiseri*, and *L. subreduncum* (Rhodophyta, Corallinales), *Phytotaxa*, 208, 183–200, <https://doi.org/10.11646/phytotaxa.208.3.1>, 2015.
- Basso, D., Babbini, L., Kaleb, S., Bracchi, V. A., and Falace, A.: Monitoring deep Mediterranean rhodolith beds, *Aquatic Conserv. Mar. Freshw. Ecosyst.*, 26, 549–561, <https://doi.org/10.1002/aqc.2586>, 2016.
- Basso, D., Babbini, L., Ramos-Esplá, A. A., and Salomidi, M.: Mediterranean rhodolith beds, in: *Rhodolith/maërl beds: A global perspective*, Springer, Cham, Coas. Res. Lib., 15, 281–298, 2017.
- Birkett, D. A., Maggs, C. A., and Dring, M. J.: An Overview of Dynamic and Sensitivity Characteristics for Conservation Management of Marine SACs, Vol. 5, *Maërl*, Scottish Association for Marine Science, Scotland, 116 pp., 1998.
- Blake, C. and Maggs, C. A.: Comparative growth rates and internal banding periodicity of maërl species (Corallinales, Rhodophyta) from northern Europe, *Phycologia*, 42, 606–612, <https://doi.org/10.2216/i0031-8884-42-6-606.1>, 2003.
- Borowitzka, M. A.: Morphological and Cytological Aspects of Algal Calcification, *Int. Rev. Cytol.*, 74, 127–162, 1982.
- Borowitzka, M. A.: Calcification in aquatic plants, *Plant Cell Environ.*, 7, 457–466, <https://doi.org/10.1111/j.1365-3040.1984.tb01436.x>, 1984.
- Borowitzka, M. A.: Carbonate calcification in algae – initiation and control, in: *Biom mineralization*, edited by: Mann, S., Webb, J., and Williams, R. J. P., Chemical and biochemical perspectives, VCH Verlagsgesellschaft, Weinheim, 63–95, 1989.
- Bracchi, V. A., Nalin, R., and Basso, D.: Morpho-structural heterogeneity of shallow-water coralligenous in a Pleistocene marine terrace (Le Castella, Italy), *Pal. Pal. Pal.*, 454, 101–112, <https://doi.org/10.1016/j.palaeo.2016.04.014>, 2014.
- Bracchi, V. A., Nalin, R., and Basso, D.: Paleocology and dynamics of coralline dominated facies during a Pleistocene transgressive–regressive cycle (Capo Colonna marine terrace, Southern Italy), *Pal. Pal. Pal.*, 414, 296–309, <https://doi.org/10.1016/j.palaeo.2014.09.016>, 2016.
- Burdett, H., Kamenos, N. A., and Law, A.: Using coralline algae to understand historic marine cloud cover, *Palaeogeogr. Palaeoclimatol.*, 302, 65–70, <https://doi.org/10.1016/j.palaeo.2010.07.027>, 2011.
- Cabioch, J. and Giraud, G.: Structural aspects of biomineralization in the coralline algae (calcified Rhodophyceae), in: *Biom mineralization in lower plants and animals*, edited by: Leadbeater, B. S. C. and Riding, R., Clarendon Press, Oxford, 141–156, 1986.
- Caragnano, A., Colombo, F., Rodondi, G., and Basso, D.: 3-D distribution of nongeniculate corallinales: a case study from a reef crest of South Sinai (Red Sea, Egypt), *Coral Reefs*, 28, 881–891, <https://doi.org/10.1007/s00338-009-0524-6>, 2009.
- Caragnano, A., Foetisch, A., Maneveldt, G. W., Millet, L., Liu, L. C., Lin, S. M., Rodondi, G., and Payri, C. E.: Revision of Corallinaceae (Corallinales, Rhodophyta): recognizing *Dawsoniolithon* gen. nov., *Parvicellularium* gen. nov. and *Chamberlainoidea* subfam. nov. containing *Chamberlainium* gen. nov. and *Pneophyllum*, *J. Phycol.*, 54, 391–409, <https://doi.org/10.1111/jpy.12644>, 2018.
- Carro, B., Lopez, L., Peña, V., Bárbara, I., and Barreiro, R.: DNA barcoding allows the accurate assessment of European maërl diversity: a Proof-of-Concept study, *Phytotaxa*, 190, 176–189, <https://doi.org/10.11646/phytotaxa.190.1.12>, 2014.
- Costa, I. O., Jesus, P. B. D., de Jesus, T. D. S., Souza, P. D. S., Horta, P. A., and Nunes, J. M. D. C.: Reef-building coralline algae from the Southwest Atlantic: filling gaps with the recognition of *Harveyolithon* (Corallinaceae, Rhodophyta) on the Brazilian coast, *J. Phycol.*, 55, 1370–1385, <https://doi.org/10.1111/jpy.12917>, 2019.
- Crouan, P. L. and Crouan, H. M.: *Florule du Finistère*, 151, pl. 20, figs 8–10, Paris and Brest, 1867.
- de Carvalho, R. T., Salgado, L. T., Amado Filho, G. M., Leal, R. N., Werckmann, J., Linhares Rossi, A., Porto Carreiro Campos, A., Santiago Karez, C., and Farina, M.: Biomineralization of calcium carbonate in the cell wall of *Lithothamnion crispatum* (Hapalidiales, Rhodophyta): correlation between the organic matrix and the mineral phase, *J. Phycol.*, 53, 642–651, <https://doi.org/10.1111/jpy.12526>, 2017.
- Flajs, G.: *Skeletal structures of some calcifying algae*, edited by: Flügel, E., *Fossil Algae: Recent Results and Developments*, Springer Berlin Heidelberg, 225–231, 1977.
- Foslie, M.: *Algologiske notiser VI*. Kongelige Norske Videnskabers Selskabs Skrifter, 1909, 1–63, 1909.
- Foster, M.: Rhodoliths: between rocks and soft places, *J. Phycol.*, 37, 659–667, <https://doi.org/10.1046/j.1529-8817.2001.00195.x>, 2001.
- Gambi, M. C., Buia, M. C., Massa-Gallucci, A., Cigliano, M., Lattanzi, L., and Patti, F. P.: The “pink mile”: benthic assemblages of rhodolith and maërl beds (Corallinales) off the Island of Ischia (Tyrrhenian Sea), in: *UNEP-MAP-RAC/SPA, Proceedings of the 1st Mediterranean Symposium on the Conservation of the Coralligenous and Other Calcareous Bio-concretions (Tabarka, 15-16/1/2009)*, edited by: Pergent-Martini, C. and Brichet, M., 198–201, 2009.
- Giraud, G. and Cabioch, J.: Aspects ultrastructuraux de la calcification chez les Corallinacées (Rhodophycées), *J. Microscopie*, 26, 14a–14a, 1976.
- Giraud, G. and Cabioch, J.: Ultrastructure and elaboration of calcified cell-walls in the coralline algae (Rhodophyta, Cryptonemiales), *Biologie Cell*, 36, 81–86, 1979.
- Halfar, J., Zack, T., Kronz, A., and Zachos, J.C.: Growth and high-resolution paleoenvironmental signals of rhodoliths (coralline red algae): A new biogenic archive, *J. Geophys. Res.-Ocean.*, 105, 22107–22116, <https://doi.org/10.1029/1999jc000128>, 2000.
- Henrich, R., Freiwald, A., Betzler, C., Bader, B., and Schäfer, P.: Controls on modern carbonate sedimentation on warm-temperate to arctic coasts, shelves, and seamounts in the Northern Hemisphere: Implications for fossil counterparts, *Facies*, 32, 71–108, <https://doi.org/10.1007/BF02536865>, 1995.
- Hernandez-Kantun, J. J., Hall-Spencer, J. M., Grall, J., Adey, W., Rindi, F., Maggs, C. A., Bárbara, I., and Peña, V.: North Atlantic Rhodolith Beds, in: *Rhodolith/Maërl Beds: A Global Perspective*, edited by: Riosmena-Rodríguez, R., Nelson, W., and Aguirre, J., Coastal Research Library, Vol. 15, Springer, Cham, [https://doi.org/10.1007/978-3-319-29315-8\\_10](https://doi.org/10.1007/978-3-319-29315-8_10), 2017.

- Huvé, H.: Contribution à l'étude des fonds à *Lithothamnium* (?) *solutum* Foslie (= *Lithophyllum solutum* (Foslie) Lemoine) de la région de Marseille, Recueil des Travaux de la Station Marine d'Endoume, 18, 105–133, 1956.
- Irvine, L. M. and Chamberlain, Y. M.: Seaweeds of the British Isles, Vol. 1, Rhodophyta Part 2B Corallinales, Hildenbrandiales, HMSO, London, 1994.
- Jacquotte, R.: Étude des fonds de maërl de Méditerranée, Recueil des Travaux de la Station Marine d'Endoume, Recueil de Travaux de la Station Marine d'Endoume, 26, 141–235, 1962.
- Kamenos, N. A. and Law, A.: Temperature controls on coralline algal skeletal growth, *J. Phycol.*, 46, 331–335, <https://doi.org/10.1111/j.1529-8817.2009.00780.x>, 2010.
- Lowenstam, H. A.: Mineral formed by organism, *Science*, 211, 1126–1131, <https://doi.org/10.1126/science.7008198>, 1981.
- Marchese, F., Bracchi, V.A., Lisi, G., Basso, D., Corselli, C., and Savini, A.: Assessing Fine-Scale Distribution and Volume of Mediterranean Algal Reefs through Terrain Analysis of Multibeam Bathymetric Data. A Case Study in the Southern Adriatic Continental Shelf, *Water*, 12, 157, <https://doi.org/10.3390/w12010157>, 2020.
- Martin, S., Castets, M. D., and Clavier, J.: Primary production, respiration and calcification of the temperate free-living coralline alga, *Aquat. Bot.*, 85, 121–128, 2006.
- Melbourne, L. A., Hernández-Kantún, J. J., Russell, S., and Brodie, J.: There is more to maerl than meets the eye: DNA barcoding reveals a new species in Britain, *Lithothamnion erinaceum* sp. nov. (Hapalidiales, Rhodophyta), *Eur. J. Phycol.*, 52, 166–178, <https://doi.org/10.1080/09670262.2016.1269953>, 2017.
- Nash, M. C. and Adey, W.: Multiple phases of mg-calcite in crustose coralline algae suggest caution for temperature proxy and ocean acidification assessment: lessons from the ultrastructure and biomineralization in *Phymatolithon* (Rhodophyta, Corallinales), *J. Phycol.*, 53, 970–984, <https://doi.org/10.1111/jpy.12559>, 2017.
- Nash, M. C., Opydyke, B. N., Troitzsch, U., Russell, B. D., Adey, W. H., Kato, A., Diaz-Pulido, G., Brent, C., Gardner, M., Prichard, J., and Kline D. I.: Dolomite-rich coralline algae in reefs resist dissolution in acidified conditions, *Nat. Clim. Change*, 3, 268–272, 2013.
- Nash, M. C., Russell, B. D., Dixon, K. R. Liu, M., and Xu, H.: Discovery of the mineral brucite (magnesium hydroxide) in the tropical calcifying alga *Polystrata dura* (Peyssonneliales, Rhodophyta), *J. Phycol.*, 51, 403–4077, <https://doi.org/10.1111/jpy.12299>, 2015.
- Nash, M. C., Diaz-Pulido, G., Harvey, A. S., and Adey, W.: Coralline algal calcification: A morphological and process-based understanding, *PLoS ONE*, 14, e0221396, <https://doi.org/10.1371/journal.pone.0221396>, 2019.
- Nothdurft, L. K. and Webb, H. E.: Earliest diagenesis in scleractinian coral skeletons: implications for palaeoclimate-sensitive geochemical archives, *Facies*, 55, 161–201, <https://doi.org/10.1007/s10347-008-0167-z>, 2008.
- Peña, V. and Bárbara, I.: Maerl community in the north-western Iberian Peninsula: a review of floristic studies and long-term changes, *Aq. Cons.-Mar. Freshw. Ecos.*, 18, 339–366, <https://doi.org/10.1002/aqc.847>, 2008.
- Peña, V. and Bárbara, I.: Distribution of the Galician maerl beds and their shape classes (Atlantic Iberian Peninsula): proposal of areas in future conservation actions, *Cahier Biol. Mar.*, 50, 353–368, 2009.
- Peña, V., Bárbara, I., Grall, J., Maggs, C. A., and Hall-Spencer, J. M.: The diversity of seaweeds on maerl in the NE Atlantic, *Mar. Biodiv.*, 44, 533–551, <https://doi.org/10.1007/s12526-014-0214-7>, 2014.
- Potin, P., Floch, J. Y., Augris, C., and Cabioch, J.: Annual growth rate of the calcareous red alga *Lithothamnion corallioides* (Corallinales, Rhodophyta) in the Bay of Brest, France, *Hydrobiologia*, 204, 263–267, <https://doi.org/10.1007/BF00040243>, 1990.
- Quaranta, F., Vannucci, G., and Basso, D.: *Neogoniolithon contii* comb. nov. based on the taxonomic re-assessment of Mastrotilli's original collections from the Oligocene of NW Italy (Tertiary Piedmont Basin), *Riv. It. Paleont. Strat.*, 113, 43–55, <https://doi.org/10.13130/2039-4942/6357>, 2007.
- Ragazzola, F., Foster, L. C., Jones, C. J., Scott, T. B., Fietzke, J., Kilburn, M. R., and Schmidt, D. N.: Impact of high CO<sub>2</sub> on the geochemistry of the coralline algae *Lithothamnion glaciale*, *Sci. Rep.*, 6, 20572, <https://doi.org/10.1038/srep20572>, 2016.
- Ragazzola, F., Caragnano, A., Basso, D., Schmidt, D. N., and Fietzke, J.: Establishing temperate crustose early Holocene coralline algae as archives for paleoenvironmental reconstructions of the shallow water habitats of the Mediterranean Sea, *Palaeontology*, 63, 155–170, <https://doi.org/10.1111/pala.12447>, 2020.
- Rashid, R., Eisenhauer, A., Liebetrau, V., Fietzke, J., Böhm, F., Wall, M., Krause, S., Rüggeberg, A., Dullo, W.C., Jurikova, H., Samankassou, E., and Lazar, B.: Early Diagenetic Imprint on Temperature Proxies in Holocene Corals: A Case Study from French Polynesia, *Front. Earth Sci.*, 8, 301, <https://doi.org/10.3389/feart.2020.00301>, 2020.
- Ries, J. B.: Mg fractionation in crustose coralline algae: Geochemical, biological, and sedimentological implications of secular variation in the Mg/Ca ratio of seawater, *Geochim. Cosmoch. Acta.*, 70, 891–900, <https://doi.org/10.1016/j.gca.2005.10.025>, 2006.
- Savini, A., Basso, D., Bracchi, V. A., Corselli, C., and Pennetta, M.: Maerl-bed mapping and carbonate quantification on submerged terraces offshores the Cilento peninsula (Tyrrhenian Sea, Italy), *Geodiversitas*, 34, 77–98, <https://doi.org/10.5252/g2012n1a5>, 2012.
- Steller, D. L., Hernández-Ayón, J. M., Riosmena-Rodríguez, R., and Cabello-Pasini, A.: Effect of temperature on photosynthesis, growth, and calcification rates of the free-living coralline alga *Lithophyllum margaritae*, *Cienc. Mar.*, 33, 441–456, <https://doi.org/10.7773/cm.v33i4.1255>, 2007.
- Vásquez-Elizondo, R. M. and Enríquez, S.: Light Absorption in Coralline Algae (Rhodophyta): A Morphological and Functional Approach to Understanding Species Distribution in a Coral Reef Lagoon, *Front. Mar. Sci.*, 4, 297, <https://doi.org/10.3389/fmars.2017.00297>, 2017.
- Wilson, S., Blake, C., Berges, J. A., and Maggs, C. A.: Environmental tolerances of free-living coralline algae (maerl): implications for European marine conservation, *Biol. Cons.*, 120, 279–289, <https://doi.org/10.1016/j.biocon.2004.03.001>, 2004.
- Woelkerling, W. J. and Irvine, L. M.: The typification and status of *Phymatolithon* (Corallinales, Rhodophyta), *British Phycol. J.*, 21, 55–80, 1986.
- Woelkerling, W. J.: The coralline red algae: an analysis of the genera and subfamilies of non-geniculate Corallinales, *British Mu-*

seum (Natural History) and Oxford University Press, London, UK, 268 pp., 1988.

Zuo, H., Balmaseda, M. A., Tietsche, S., Mogensen, K., and Mayer, M.: The ECMWF operational ensemble reanalysis–analysis system for ocean and sea ice: a description of the system and assessment, *Ocean Sci.*, 15, 779–808, <https://doi.org/10.5194/os-15-779-2019>, 2019.